Propulsion in hexapod locomotion: How do desert ants traverse slopes?

Toni Wöhrl, Lars Reinhardt and Reinhard Blickhan

Abstract

The employment of an alternating tripod gait to traverse uneven terrains is a common characteristic shared among many hexapoda. Since this could be one specific cause for their ecological success, we examined the alternating tripod gait of the desert ant *Cataglyphis fortis* together with their ground reaction forces and weight-specific leg impulses for level locomotion and on moderate (±30°) and steep (±60°) slopes in order to understand mechanical functions of individual legs during inclined locomotion. Based on the experimental data, it was proposed that 1) the hind legs acted as the main brake (negative weight-specific impulse in the direction of progression) on both the moderate and steep downslopes while the front legs became the main motor (positive weight-specific impulse in the direction of progression) on the steep upslope. In both cases the primary motor or brake was found to be above the centre of mass. 2) Normalised double support durations were prolonged on steep slopes, which could enhance the effect of lateral shear loading between left and right legs with the presence of direction-dependent attachment structures. 3) The notable directional change in the lateral ground reaction forces between the moderate and steep slopes implied the utilisation of different coordination programs in the extensor-flexor system.

Keywords

Alternating Tripod Gait, Attachment, Ground reaction force, Impulse, Navigation, Stability

List of symbols and abbreviations

l	Leg number l = {(1,front), (2,middle), (3,hind)}
k	Direction k = {(x, fore-aft, direction of progression), (y, lateral, left-right), (z, normal to the substrate)}
GRF	Ground reaction force
CoM	Center of mass
BW	Unit body weight
J_{lk}	Weight-specific leg impulse $J_{lk} = (mg)^{-1} \cdot \int F_{lk}(t)dt$: GRF F_{lk} integrated over the time of foot contact for each leg and direction divided by the body weight (body mass m times the local acceleration of free fall g = $9.81 ms^{-2}$)
t_{ll}	Normalised double support durations for each leg pair from the touchdowns of one tripod composition (left front leg L1, right middle leg R2, left hind leg L3) to the subsequent lift-offs of the other tripod composition (R1, L2, R3) normalised by the stride durations of the middle legs.

Introduction

Ants possess a large set of motor skills, such as moving within confined spaces in the soil (Gravish et al., 2013), traversing slopes (Seidl and Wehner, 2008; Weihmann and Blickhan, 2009), climbing (Endlein and Federle, 2015), swimming (Bohn et al., 2012) and even gliding (Yanoviak et al., 2005). Despite their wide range of body weights, which varies approximately from 0.008 mg (Kaspari and Weiser, 1999) to 480 mg (Linsenmair, 1998), the ants as a family have adopted a common motion system that enabled the lightest species to manoeuvre in a surface-dominated micro environment where molecular forces predominate, and the heaviest species to prevail in a volume-dominated macro environment where gravitational forces exceed molecular forces (Went, 1968).

One of the primary characteristics of their motion system is the alternating tripod gait, which was identified to be a relatively robust locomotion pattern for hexapoda in different settings (e.g. Seidl and Wehner, 2008; Wahl et al., 2015; Zollikofer, 1994a,b,c) and probably helped them to conquer various habitats. Since traversing slopes and climbing belong to the very basic routine of many worker ants, previous studies have already described either their kinematics over different inclines or their kinematics and forces for level locomotion and vertical climbing. For example, a kinematic study on desert ants found that the ground contact durations changed with the inclination of the slope, whereas the positioning of the legs was independent of the slope (Seidl and Wehner, 2008). Other studies have combined kinematics and forces and observed that wood ants and other hexapoda such as cockroaches and stick insects pushed with both their front and hind legs for level locomotion (Cruse, 1976; Full et al., 1991; Reinhardt and Blickhan, 2014a), and identified the influence of surface on interactions between (pre) tarsal structures of weaver ants for level locomotion (Endlein and Federle, 2008). A separate study on vertically climbing weaver ants on a smooth surface found that the legs above the centre of mass (CoM) mainly held their body weight (Endlein and Federle, 2015). In order to overcome gravity and climb upward, their front legs used more pulling forces than the pushing forces of the hind legs in the fore-aft direction, while in climbing downward, their hind legs used more pulling forces than the pushing forces of the front legs. It was then concluded that weaver ants mainly utilised the distal-located *arolia* for pulling and the more proximally-located 3rd and 4th *tarsomeres* for pushing (Endlein and Federle, 2015).

A modelling study for a three-point climber with cockroach geometry has predicted that the slope angle for the push-pull transition of the front legs in the normal direction of the substrate could be increased from around 40° to 70° by lowering down the relative height (body height per body length) from 0.2 to 0.1 (Günther and Weihmann, 2012). However, the transition between the pushing of the front and hind legs on level locomotion and the pulling by legs above the CoM on vertical climbing

has not been supported with experimental data for any kind of hexapod yet. Therefore, the present study firstly examined the changes in the alternating tripod gait and ground reaction forces (GRF) of *Cataglyphis fortis* on different slopes to describe the kinematics and forces of ants during inclined locomotion.

In addition, we calculated the weight-specific leg impulses, which are the integrals of GRF over the time of foot contacts normalised by the body weight for each leg and direction, to determine the impact of individual legs on propulsion and load over stride cycles. While kinematic and GRF data can identify leg actions such as pulling (GRF vector points from the tarsi away from the CoM) and pushing (GRF vector points from the tarsi towards the CoM) at every point of time, they might not be sufficient to determine which pair of legs pulls or pushes the animals the most within one stride cycle in multi-legged locomotion. This is because one leg could generate relatively high force peaks for a short time (high average force), but its pulling or pushing impact on propulsion and load could still be less than the other leg if the latter had lower forces for a longer time (low average force). In such cases, calculating the weight-specific leg impulses becomes crucial in pinpointing mechanical functions of individual legs, where a positive weight-specific impulse in the direction of progression (fore-aft) indicates the function of a motor, and a negative weight-specific impulse indicates the function of a brake.

Thus, in order to study mechanical functions of individual hexapod legs over inclined locomotion, the present study has focused on how the alternating tripod gait, the GRF and the weight-specific leg impulses of the desert ant *Cataglyphis fortis* changed on different slopes. Since the load carrying functions of the leg pairs have been studied for vertical climbing weaver ants on a smooth surface (Endlein and Federle, 2015), where the font legs used more pulling forces in climbing upward and the hind legs used more pulling forces in climbing downward, it was hypothesised that for the transition between level locomotion and vertical climbing, the front legs of *Cataglyphis* exerted pulling forces as the dominant motor on upslopes whereas the hind legs exerted pulling forces as the dominant brake on downslopes.

Methods

Animals

A *Cataglyphis fortis* colony with more than 600 ants from Tunisia near Menzel Chaker was housed in a formicarium. A 60 W daylight lamp was installed to illuminate one half of the formicarium from 7 am to 7 pm. The temperature of the formicarium was kept at around 28°C. The ants were fed with honey, water and insects *ad libitum*. The experiments were performed between October 2012 and March 2013 at Friedrich Schiller University Jena.

Data acquisition

We used the same experimental setup and procedure as previously published by our work group (Reinhardt and Blickhan, 2014b,a). For each set of measurement, one ant was randomly taken from the formicarium with a plastic tube (diameter 12 mm, length 150 mm) and repeatedly placed at the start of a 90 mm long running track. The running track was covered with graph paper and confined to a width of 25 mm and a height of 30 mm.

A custom-built three-dimensional 4 x 4 mm force platform with resolvable forces $F_x = 5.4\mu N$, $F_y = 2.9\mu N$, $F_z = 10.8\mu N$ (Reinhardt and Blickhan, 2014b) was fixed in the middle of the track and also covered with graph paper. It was designed based on PVC/semiconductor strain gauges KSP-3-120-F2-11 (Kyowa, Tokyo, Japan) and used to record the GRF of single steps of the moving ants. The signals received by the force platform were amplified by a data acquisition system (MGCplus, Hottinger Baldwin Messtechnik, Darmstadt, Germany) and collected by a computer with a sampling frequency of 1200 Hz. The natural frequencies of the force platform with the graph paper attached were measured to be $f_x = 380Hz$, $f_y = 279Hz$ and $f_z = 201Hz$. The force data could not be used to identify the dragging length because the dragging forces were smaller than the resolvable forces and the ants could drag their legs off the force platform.

A Photron Fastcam SA3 (San Diego, CA, USA) camera with a frequency of 500 Hz was used to record the dorsal view of the ants. The sagittal view was captured by the same camera objective via glass prisms functioning as a 45° mirror. MATLAB R20015b (The MathWorks, Inc., USA) and DigitizingTools 20160711 (Hedrick, 2008) were used for motion tracking.

The body masses of the ants were measured with a precision scale (±0.1 mg, ABS 80-4, Kern & Sohn, Germany) directly after each single leg force signal was recorded. After each set of measurement, the investigated ant was isolated in a separate box and only placed back to the formicarium at the end of every measurement day.

Data selection

A total of 893 trials with GRF measurements and video sequences were recorded. In the first round of data screening, we excluded trials where the ants stopped, changed direction or touched the force platform with their gasters. Trials where the ants dragged their hind legs were not excluded from the dataset.

Subsequently, we took the first 15 force and kinematic measurements for each set of legs (front legs, middle legs, hind legs) and slope (steep=±60°, moderate=±30, 0°) for further data analysis. Altogether, 225 different strides from 225 different runs were selected.

Data analysis

MATLAB 8.6.0 R20015b (The MathWorks, Inc., USA) and R 3.3.1 were used for data analysis. Petiole and tarsi trajectories and the GRF were calculated over one stride cycle i.e. consecutive touchdowns of the same leg and adjusted to the average direction of progression through rotational transformation in the frontal xy-plane. The kinematic and force signals were smoothed with a Savitzky-Golay filter (window size of 5). All signals were normalised to the body weight and the mean stepping pattern for every slope (45 strides per slope). The GRF were given in arithmetic means and standard deviations unless stated otherwise.

The GRF signals were extrapolated with the assumptions that 1) the GRF did not change over multiple stride cycles, i.e. straight locomotion and constant speed; 2) left and right leg GRF were mirrored in the lateral direction and equal in the normal and fore-aft direction, i.e. bilateral symmetry of GRF and tripod symmetry of the ant body. As a result, the GRF signals were periodic.

The weight-specific leg impulses were approximated numerically using the trapezoidal sum method with partitions of equal size $\Delta t = 1200^{-1} s$ of the GRF over the whole ground contact duration.

The Wilcoxon rank sum test with Bonferroni correction was used to compare the measurements.

Results

Actuation on upslopes

On the moderate upslope, the primary motor of *Cataglyphis* (Fig. 1A, Table 1) were found to be the middle and hind legs as $J_{1x}(30°) < J_{2x}(30°)$ (p<0.01) and $J_{1x}(30°) < J_{3x}(30°)$(p<0.01). Pushing forces by the hind legs dominated over pulling forces by the front legs, where the CoM was mostly above the tarsi (Fig. 2D). On the steep upslope, the primary motor became the front legs as $J_{1x}(60°) > J_{2x}(60°)$(p<0.001) and $J_{1x}(60°) > J_{3x}(60°)$(p<0.001). Pulling forces by the front legs above the CoM

dominated over pushing forces by the hind legs below the CoM (Fig. 2E). The front legs exhibited the highest amplitude of the mean GRF at about $F_{1x}(60°) \approx 0.5\text{BW} \approx 120\mu N$(Fig. 3A).

In the sagittal view (xz-plane), the mean GRF vectors of the hind legs pointed along the tibia axis towards the gaster on both the moderate and steep upslopes (Fig. 2D,E). In the dorsal view (xy-plane), they pointed into the area of the supporting tripod towards the CoM, whereas front and middle leg GRF vectors pointed out of the supporting tripod frame. All legs pushed outwards on the moderate upslope (Fig. 2D), but a directional change in the lateral GRF occurred for the front legs on the steep upslope as they started pulling inwards (Fig. 2E). The GRF standard deviations were observed to increase on the steep upslope for all leg pairs (Fig. 3A).

The shapes of the GRF over time changed remarkably from the moderate to steep upslope for the front and hind legs in the normal direction. Whereas front leg GRF diminished on the steep upslope, hind leg GRF changed from a triangular shape on the moderate upslope to a trapezoidal shape with longer double support durations on the steep upslope.

Braking on downslopes

Hind legs were used as the primary braking unit for both the moderate and steep downslopes as $J_{3x}(-30°) < J_{2x}(-30°) < 0$(p<0.05), $J_{3x}(-30°) < J_{1x}(-30°) < 0$ (p<0.001), $J_{3x}(-60°) < J_{2x}(-60°) < 0$(p<0.001) and $J_{3x}(-60°) < J_{1x}(-60°) < 0$ (p<0.001) (Fig. 1A, Table 1). Pulling forces by the hind legs above the CoM dominated over pushing forces by the front and middle legs below the CoM (Fig. 2A,B). The hind legs on the steep downslope had the strongest mean GRF at about $F_{3x}(-60°) \approx -0.5\text{BW} \approx -120\mu N$ (Fig. 3A).

In the sagittal view, braking forces of the front legs pointed along the tibia axis towards the head (Fig. 2A,B). In the dorsal view, they pointed into the area of the supporting tripod towards the thorax.

Similar to the shift in direction in the lateral GRF of the front legs on the steep upslope, the hind legs started pulling strongly inwards on the steep downslope (Figs 1A,2A).

Direction-dependency

A comparison of impulses on the steep upslope against the steep downslope for the same leg pair revealed that front legs pulled more strongly on the steep upslope than they pushed on the steep downslope (Fig. 1A) as $|J_{1x}(-60°)| < |J_{1x}(60°)|$ (p<0.001). Similarly, hind leg pulling impulses were stronger on the steep downslope than pushing impulses on the steep upslope as $|J_{3x}(60°)| < |J_{3x}(-60°)|$ (p<0.05).

Front-hind leg symmetry

The GRF vectors of the front legs on upslopes (Fig. 4A-D, dark blue arrows) were compared against those of the hind legs on downslopes (light red arrows). At the same time, the GRF vectors of the front legs on downslopes (light blue arrows) were also compared against those of the hind legs on upslopes (dark red arrows). Even though the starting points of the GRF vectors were more distal for the hind legs than for the front legs, it was observed that the GRF vectors of the front legs on the steep upslope and those of the hind legs on the steep downslope (Fig. 4A,B) had similar magnitudes but had opposite directions along the body (x) axis, and vice versa. Such symmetry was also evident on moderate slopes (Fig. 4C,D), although there was slight deviation in the direction of the GRF vectors of the hind legs in the lateral direction on the moderate downslope.

In the fore-aft direction, front and hind legs exhibited supportive mechanical functions during inclined locomotion as $sgn\big(J_{1x}(\neg0°)\big) = sgn\big(J_{3x}(\neg0°)\big)$ and contrary mechanical functions for level locomotion as $sgn\big(J_{1x}(0°)\big) \neq sgn\big(J_{3x}(0°)\big)$. While the distribution of the body weight in the normal direction was nearly equal for level locomotion among the three leg pairs, it was shifted mostly to the hind leg on the steep upslope and to the front and middle legs on the steep downslope (Figs 1C, 2A-E).

Dragging hind leg

The hind legs were dragged behind the ants in numerous measurements. In order to distinguish aerial phases from dragging, we set the maximum height of uncertainty to 0.4 mm which was twice the magnitude of the measuring accuracy. The number of lift-offs were counted and the dragging length for each slope was calculated (Fig. 5A, Table 2). The median dragging length ranged from 2.2 mm (moderate upslope) to 5.6 mm (steep downslope) and constituted 26 % to 82 % of the step length depending on the slope. Most of the dragging across the whole swing phase occurred on the steep downslope, which was observed in 67 % of all steep downslope strides.

Total GRF over time

In order to ensure the validity of the measurements, the total GRF over time was calculated for all six legs on all slopes (Table 3). In the ideal case, the total GRF in the normal direction should oscillate at around a mean of 1 BW for level locomotion, $\sqrt{3} \cdot 2^{-1}$BW at ±30° slope, and 2^{-1} BW at ±60° slope. However, the calculated total GRF over multiple stride cycles were 0.03 BW (moderate downslope) to 0.10 BW (level locomotion) lower than the ideal case. This could be attributed to the dragging hind leg (Fig. 4, Table 2), which could have generated pulling or pushing forces during the dragging phase.

Kinematics

Temporal parameters such as ground contact duration and running speed were highly variable across all slopes (Table 4). For example, the standard deviations of the contact durations of the middle legs increased from 11 ms for level locomotion to 29 ms on the steep downslope. The mean speed ranged from 54 ± 10 mm s^{-1} (steep upslope) to 87 ± 17 mm s^{-1} (level locomotion). The duty factor of the middle legs lay between 62 ± 9 % (moderate downlsope) and 72 ± 7 % (steep downslope). The body height (CoM-substrate distance, Table 4 and Fig. 5B) ranged from 2.4 ± 0.4 mm (steep downslope) to 3.8 ± 0.7 mm (level locomotion).

Touchdowns and lift-offs of the tripod composition occurred almost simultaneously on the moderate slopes and level locomotion. However, the tarsi of the left hind legs touched down and lifted off the ground later than the right middle legs and left front legs on the steep slopes, and vice versa (Fig. 3A,B,C). The normalised double support durations (Fig. 6) increased significantly for the front ($p<0.001$) and hind legs ($p<0.001$) from level locomotion to the steep upslope and for the middle legs from level locomotion to the steep slopes ($p<0.01$).

Discussion

Motor and brake functions

Similar to the findings about vertically climbing weaver ants on a smooth surface, where a larger proportion of body weight was carried by the legs above the CoM (Endlein and Federle, 2015), our measurements showed that the front legs rose above the CoM and became the primary motor (positive weight-specific leg impulse in the direction of progression) on the steep upslope. The hind legs maintained their position above the CoM and kept their function as the primary braking leg pair (negative weight-specific leg impulse in the direction of progression) on both the moderate and steep downslopes. While the dominant braking function of the hind legs on downslopes corresponded with our hypothesis, the front legs did not act as the primary motor on the moderate upslope probably because the tarsi did not rise above the CoM adequately (Fig. 2). Therefore, we deduced that the position of the tarsi relative to the CoM could be the main factor in determining the individual leg pairs as the primary motor or brake during inclined locomotion.

This suggested that the tarsi of the front legs could act as the main suspension point of the supporting tripod on the steep upslope and the tarsi of the hind legs could act as the main suspension point on downslopes. If the hind legs were used as the primary motor on the steep upslope, the main suspension point would be below the CoM, thereby causing instability. Further stability could be achieved by the dragging hind leg. Under risky situations such as moving down the steep slope where most of the dragging across the whole swing phase was observed, the dragging leg could form a temporary quadrangle configuration or hook onto protruding objects for abrupt braking.

Direction-dependency and shear loading

The front and hind legs also showed direction-dependent GRF and weight-specific impulses. For the front legs, the fore-aft pulling impulses (motor function) on the steep upslope were higher than their pushing impulses (brake function) on the steep downslope. For the hind legs, the fore-aft pulling impulses (brake function) on the steep downslope were higher than their pushing impulses (motor function) on the steep upslope. In the lateral direction, the front legs changed from pushing outwards to pulling inwards from the moderate to the steep upslope whereas the hind legs changed from pushing outwards to pulling inwards from the moderate to the steep downslope.

Higher pulling forces over pushing forces were observed in other hexapoda as well, including stick insects, cockroaches and ants (Bullock et al., 2008; Clemente and Federle, 2008; Endlein and Federle, 2015). Close examination of the silhouettes of the typical tarsus of *Cataglyphis*, hornets and weaver ants (Frantsevich and Gorb

2004; Endlein and Federle, 2008) revealed that the claws of their front legs were curved against the direction of progression, but those of their hind legs were curved towards the direction of progression. As such, the action of pulling for both the front and hind legs would be able to help the ants interlock their claws better with the surface asperities of our substrate. This could be of special importance for *Cataglyphis* considering the granular surface of their desert habitat.

The presence of direction-dependent attachment structures could also enhance shear loading of the opposing tarsi of the ants. Just as shear loading of the opposing toes or legs enabled geckos to hang from the ceiling (Autumn, 2006) and spiders to make use of the collective effect of their hairy foot pads (Wohlfart et al., 2014), it could also help the ants to move on steep surfaces. The increase in the normalised durations of double support phases from level locomotion to steep slopes in the experiment implied that the forces in the lateral direction acted longer against each other on steep slopes (Fig. 3B). Thus, by changing their temporal gait kinematics, the ants could engage their opposing tarsal hair structures and probably adjust their whole body adhesion force to move on steep surfaces.

Coordination and navigation

The changes in the weight-specific leg impulses as well as the changes of the magnitudes and directions of the GRF over time and different slopes could imply that the ants employed different coordination programs in their extensor-flexor system on different slopes. For example, the front legs switched from pushing to pulling laterally between the moderate and steep upslope, whereas the hind legs switched from pushing to pulling laterally between the moderate and steep downslope. This showed that the participating muscles and their interactions could have changed with the slope.

Such changes could further provide insights into the mechanisms behind hexapod navigation. *Cataglyphis* were found to employ odometry during inclined locomotion (Wittlinger et al., 2006; Wohlgemuth et al., 2001) and it had been suggested that both odometry and gravity perception could play a key role in their three-dimensional path integration. However, the primary receptors in gravity perception for *Formica,* the hair fields located on the body joints (Markl, 1962; Markl, 1974), were not necessary for path integration of *Cataglyphis* (Wittlinger et al., 2007), neither was the monitoring of the thorax-coxae joint angles. Instead, force sensors such as muscular strain sensors and *campaniform sensilla* could provide idiothetic cues for three-dimensional path integration (Seidl and Wehner, 2008). Such sense organs exhibited orientation-dependent directional sensitivity (Zill and Moran, 1981) and have been observed in other hexapoda such as cockroaches (e.g. McIver, 1975; Moran et al., 1971; Pringle, 1938; Ridgel et al., 2000) and stick insects (e.g. Schmitz, 1993; Zill et al., 2013).

Even though we could not verify the involvement of proprioceptors in path integration directly from the results, it was clear that the strain on the attachment structures and leg segments has changed on different slopes due to the changes in the magnitudes and directions of the GRF. If similar patterns of GRF changes could be observed on a different substrate or with another ant species, it would be possible to hypothesise that ants triggered a relatively consistent motor program with respect to the angle of the slope, where the cuticular structures were affected more by the slope of the substrate than its roughness or stiffness. As such, the bending of leg segments or tarsi during inclined locomotion could probably be discussed together with odometry in three-dimensional path integration of *Cataglyphis*.

Summary

In the analysis of mechanical functions of the individual legs of desert ants on different slopes, our experimental data showed that the tarsi of the hind legs were above the CoM and acted as the main brake on both the moderate and steep downslopes, whereas the main motor changed from the middle and hind legs at the moderate upslope to the front legs at the steep upslope after the tarsi of the front legs rose above the CoM. It suggested that the need to maintain stability during inclined locomotion always constituted the shift of the main motor/brake towards the leg pair above the CoM. This finding varied slightly from our hypothesis about the mechanical function of the front legs, which we initially surmised to be the main motor on both the moderate and steep upslopes.

The increased double support durations on steep slopes probably enhanced shear loading of the opposing tarsal hair structures to ensure better adhesion on steep surfaces. In addition, the notable change of the weight-specific leg impulses from pushing laterally on the moderate slopes to pulling laterally on the steep slopes illustrated the flexibility of the extensor-flexor system, which could serve as another potential mechanism for the path integration of the desert ants.

Acknowledgments

Competing interests

Author contributions

Funding

References

Autumn, K. (2006). Properties, principles, and parameters of the gecko adhesive system. In *Biological adhesives* (ed. A. M. Smith and J. A. Callow), pp. 225-256. Berlin, Heidelberg: Springer.

Bohn, H. F.; Thornham, D. G. and Federle, W. (2012). Ants swimming in pitcher plants: kinematics of aquatic and terrestrial locomotion in camponotus schmitzi. *J. Comp. Physiol. A* **198**, 465-476.

Bullock, J. M. R.; Drechsler, P. and Federle, W. (2008). Comparison of smooth and hairy attachment pads in insects: friction, adhesion and mechanisms for direction-dependence. *J. Exp. Biol.* **211**, 3333-3343.

Clemente, C. J. and Federle, W. (2008). Pushing versus pulling: division of labour between tarsal attachment pads in cockroaches. *Proc. R. Soc. B* **275**, 1329-1336.

Cruse, H. (1976). The function of the legs in the free walking stick insect, Carausius morosus. *J. Comp. Physiol. A* **112**, 235-262.

Endlein, T. and Federle, W. (2008). Walking on smooth or rough ground: passive control of pretarsal attachment in ants. J. Comp. Physiol. A **194**, 49-60.

Endlein, T. and Federle, W. (2015). On heels and toes: how ants climb with adhesive pads and tarsal friction hair arrays. *PLoS One* **10**, e0141269.

Frantsevich, L. and Gorb, S. (2004). Structure and mechanics of the tarsal chain in the hornet, Vespa crabro (Hymenoptera: Vespidae): implications on the attachment mechanism. *Arthropod. Struct. Dev.* **33**, 77-89.

Full, R. J.; Blickhan, R. and Ting, L. H. (1991). Leg design in hexapedal runners. *J. Exp. Biol.* **158**, 369-390.

Gravish, N.; Monaenkova, D.; Goodisman, M. A. D. and Goldman, D. I. (2013). Climbing, falling, and jamming during ant locomotion in confined environments. *Proc. Natl. Acad. Sci. USA* **110**, 9746-9751.

Günther, M. and Weihmann, T. (2012). Climbing in hexapods: A plain model for heavy slopes. *J. Theoret. Biol.* **293**, 82-86.

Hedrick, T. L. (2008). Software techniques for two- and three-dimensional kinematic measurements of biological and biomimetic systems. *Bioinspir. Biomim.* **3**, 34001.

Kaspari, M. and Weiser, M. D. (1999). The size-grain hypothesis and interspecific scaling in ants. *Funct. Ecol.* **13**, 530-538.

Linsenmair, K. E. and Pfeiffer, M. (1998). Polydomy and the organization of foraging in a colony of the Malaysian giant ant Camponotus gigas (Hym./Form.). *Oecologia.* **117**, 579-590.

Markl, H. (1962). Borstenfelder an den Gelenken als Schweresinnesorgane bei Ameisen und anderen Hymenopteren. *Z. vergl. Physiol.* **45**, 475-569.

Markl, H. (1974). The perception of gravity and of angular acceleration in invertebrates. In

Handbook of Sensory Physiology. Vestibular System Part 1: Basic Mechanisms (ed. H. H. Kornhuber), pp. 17-74. Berlin, Heidelberg: Springer.

McIver, S. B. (1975). Structure of cuticular mechanoreceptors of arthropods. *Annu. Rev. Entomol.* **20**, 381-397.

McMeeking, R. M.; Arzt, E. and Wehner, R. (2012). Cataglyphis desert ants improve their mobility by raising the gaster. *J. Theoret. Biol.* **297**, 17-25.

Moran, D. T.; Chapman, K. M. and Ellis, R. A. (1971). The fine structure of cockroach campaniform sensilla. *J. Cell Biol.* **48**, 155-173.

Pringle, J. (1938). Proprioception in insects I. A new type of mechanical receptor from the palps of the cockroach. *J. Exp. Biol.* **15**, 101-113.

Reinhardt, L. and Blickhan, R. (2014a). Level locomotion in wood ants: evidence for grounded running. *J. Exp. Biol.* **217**, 2358-2370.

Reinhardt, L. and Blickhan, R. (2014b). Ultra-miniature force plate for measuring triaxial forces in the micronewton range. *J. Exp. Biol.* **217**, 704-710.

Ridgel, A.; Frazier, S.; DiCaprio, R. and Zill, S. (2000). Encoding of forces by cockroach tibial campaniform sensilla: implications in dynamic control of posture and locomotion. *J. Comp. Physiol. A* **186**, 359-374.

Schmitz, J. (1993). Load-compensating reactions in the proximal leg joints of stick insects during standing and walking. *J. Exp. Biol.* **183**, 15-33.

Seidl, T. and Wehner, R. (2008). Walking on inclines: how do desert ants monitor slope and step length. *Front. Zool.* **5**, 1-15.

Wahl, V.; Pfeffer, S. E. and Wittlinger, M. (2015). Walking and running in the desert ant Cataglyphis fortis. *J. Comp. Physiol. A* **201**, 645-656.

Weihmann, T. and Blickhan, R. (2009). Comparing inclined locomotion in a ground-living and a climbing ant species: sagittal plane kinematics. *J. Comp. Physiol. A* **195**, 1011-1020.

Went, F. W. (1968). The size of man. Am. Sci. **56**, 400-413.

Wittlinger, M.; Wehner, R. and Wolf, H. (2006). The ant odometer: Stepping on stilts and stumps. *Science* **312**, 1965-1967.

Wittlinger, M.; Wolf, H. and Wehner, R. (2007). Hair plate mechanoreceptors associated with body segments are not necessary for three-dimensional path integration in desert ants, Cataglyphis fortis. *J. Exp. Biol.* **210**, 375-382.

Wohlfart, E.; Wolff, J. O.; Arzt, E. and Gorb, S. N. (2014). The whole is more than the sum of all its parts: collective effect of spider attachment organs. *J. Exp. Biol.* **217**, 222-224.

Wohlgemuth, S.; Ronacher, B. and Wehner, R. (2001). Ant odometry in the third dimension. *Nature* **411**, 795-798.

Yanoviak, S. P.; Dudley, R. and Kaspari, M. (2005). Directed aerial descent in canopy ants *Nature* ***433***, 624-626.

Zill, S. N.; Chaudhry, S.; Büschges, A. and Schmitz, J. (2013). Directional specificity and encoding of muscle forces and loads by stick insect tibial campaniform sensilla, including receptors with round cuticular caps. *Arthropod. Struct. Dev.* **42**, 455-467.

Zill, S. N. and Moran, D. T. (1981). The exoskeleton and insect proprioception. I. Responses of tibial campaniform sensilla to external and muscle-generated forces in the American cockroach, Periplaneta americana. *J. Exp. Biol.* **91**, 1-24.

Zollikofer, C. P. E. (1994a). Stepping patterns in ants - influence of body morphology. *J. Exp. Biol.* **192**, 107-118.

Zollikofer, C. P. E. (1994b). Stepping patterns in ants - influence of load. *J. Exp. Biol.* **192**, 119-127.

Zollikofer, C. P. E. (1994c). Stepping patterns in ants - influence of speed and curvature. *J. Exp. Biol.* **192**, 95-106.

Tables

Table 1. Inter-leg comparisons of the weight-specific leg impulses. Tested with the two-sided Wilcoxon rank sum test with Bonferroni correction (N=15 strides for each subset). i: Slope; k: Direction; N: Number of different strides; N_m: Unique masses ($\Delta m \geq 0.1$ mg); N_d: Measurement days; $N_1; N_2; N_3$: Number of different individuals for front, middle and hind leg measurements (Individuals per nest $\geq$ 600); p>0.05: ns; p≤0.05:*; p≤0.01:**; p≤0.001:***

i (deg)	k	N	N_m	N_d	$N_1; N_2; N_3$	$J_{1k} \overset{H_0}{=} J_{2k}$	$J_{1k} \overset{H_0}{=} J_{3k}$	$J_{2k} \overset{H_0}{=} J_{3k}$
-60	x	45	29	9	≤13; ≤9; ≤9	ns	***	***
-60	y	45	29	9	≤13; ≤9; ≤9	*	***	***
-60	z	45	29	9	≤13; ≤9; ≤9	**	***	***
-30	x	45	32	16	≤14; ≤10; ≤14	ns	**	*
-30	y	45	32	16	≤14; ≤10; ≤14	***	***	***
-30	z	45	32	16	≤14; ≤10; ≤14	ns	***	***
0	x	45	31	13	≤12; ≤9; ≤12	***	**	ns
0	y	45	31	13	≤12; ≤9; ≤12	***	ns	***
0	z	45	31	13	≤12; ≤9; ≤12	ns	ns	*
30	x	45	30	19	≤13; ≤12; ≤15	***	***	ns
30	y	45	30	19	≤13; ≤12; ≤15	***	ns	***
30	z	45	30	19	≤13; ≤12; ≤15	***	***	ns
60	x	45	25	8	≤10; ≤6; ≤8	***	***	ns
60	y	45	25	8	≤10; ≤6; ≤8	***	***	***
60	z	45	25	8	≤10; ≤6; ≤8	***	***	***

Table 2. Dragging hind leg measurements. I: Slope; N_{LO}: Number of lift-offs; l_3: Step length; d_3: Dragging length; $l_{3n} = d_3 l_3^{-1}$: Normalised dragging length; h_3: Tarsus lift heights; medians

I (deg)	Strides	N_{LO}	l_3(mm)	d_3(mm)	l_{3n}(%)	h_3(mm)
-60	15	5	6.8	5.6	82	0.4
-30	15	12	7.8	2.8	36	0.8
0	15	12	9.2	3.2	35	1.0
30	15	13	8.6	2.2	26	1.0
60	15	12	8.5	4.6	54	1.4

Table 3. Mean of total GRF. i: Slope; k: Direction; BW: Body weight; GRF: Ground reaction force; AE: Absolute errors

i (deg)	k	Strides	BW (μN)	Mean total GRF (BW)	AE (BW)
-60	x	45	237±40	-0.77±0.10	-0.10±0.10
-60	y	45	237±40	0.00±0.13	0.00±0.13
-60	z	45	237±40	0.41±0.04	-0.09±0.04
-30	x	45	239±37	-0.45±0.08	-0.05±0.08
-30	y	45	239±37	0.00±0.02	0.00±0.02
-30	z	45	239±37	0.83±0.10	-0.03±0.10
0	x	45	249±35	0.06±0.08	0.06±0.08
0	y	45	249±35	0.00±0.02	0.00±0.02
0	z	45	249±35	0.90±0.08	-0.10±0.08
30	x	45	232±27	0.46±0.10	-0.04±0.10
30	y	45	232±27	0.00±0.05	0.00±0.05
30	z	45	232±27	0.79±0.07	-0.07±0.07
60	x	45	232±27	0.93±0.11	0.07±0.11
60	y	45	232±27	0.00±0.09	0.00±0.09
60	z	45	232±27	0.50±0.07	0.00±0.07

Table 4. Kinematic parameter. i: Slope; t_{2s}: Stride duration of the middle legs; t_{2c}: Contact duration of the middle legs; t_{2d}: Duty factor of the middle legs; v: Running speed; s: Displacement of the CoM per stride; h_{CoM}: Body height (CoM-substrate distance); (means±s.d.; N=45 strides for each subset)

i (deg)	t_{2s}(ms)	t_{2c}(ms)	t_{2d}(%)	v (mm/s)	s (mm)	h_{CoM}(mm)
-60	128±30	93±29	72±7	64±25	7.7±1.9	2.6±0.7
-30	109±14	69±15	62±9	84±26	9.0±2.1	3.6±0.5
0	110±13	69±11	63±6	87±17	9.7±1.6	3.8±0.7
30	136±23	90±20	66±6	71±15	9.5±1.2	3.0±0.4
60	169±20	114±20	68±7	54±10	9.1±1.2	2.4±0.4

Figures
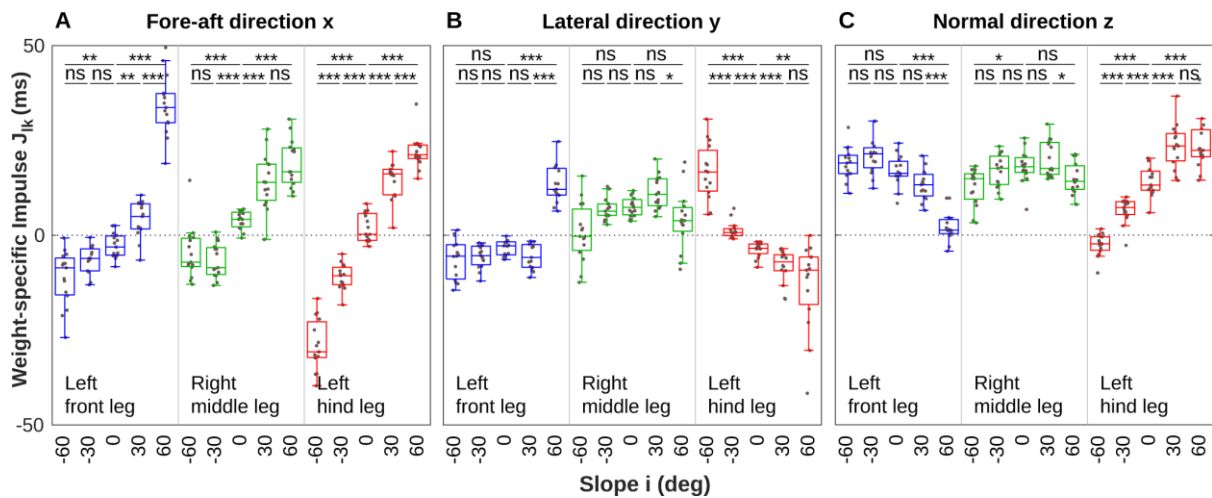
Fig. 1. Weight-specific leg impulses at different slopes. The central lines of the Tukey boxplots are the medians and the edges of the boxes are the 25th and 75th percentiles (N=15 strides for each subset). The results are grouped by the directions of the impulses (A-C) and by the type of the leg (front, middle and hind leg). $p > 0.05$: ns; $p \leq 0.05$:*; $p \leq 0.01$:**; $p \leq 0.001$:***; two-sided Wilcoxon rank sum test with Bonferroni correction.
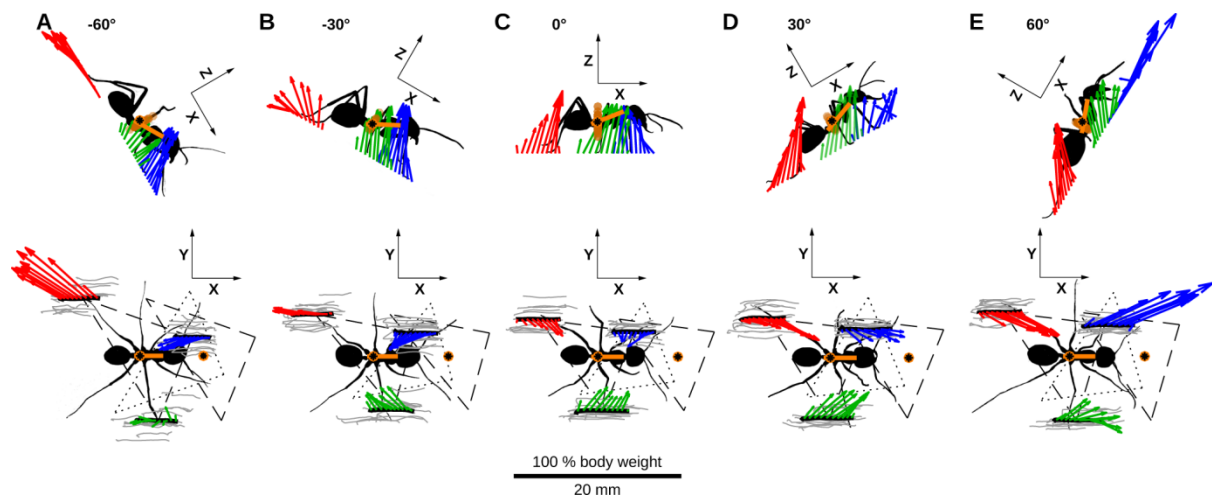
Fig. 2. Mean GRF vectors with mean stepping patterns at different slopes. (A) Steep downslope; (B) Moderate downslope; (C) Level locomotion; (D) Moderate upslope; (E) Steep upslope. The direction of progression x is from left to right. Blue, green and red arrows indicate the mean GRF vectors of left front leg, right middle leg and left hind leg respectively. GRF and tarsus trajectories are plotted in the sagittal views (xz-planes) as well as the dorsal views (xy-planes) in body-fixed coordinate systems with the origins in the CoMs. The solid grey/black lines in the xy-planes represent the measured/mean tarsus trajectories during the ground contacts from touchdowns to lift-offs (tarsus motions from right to left). The dashed and dotted black triangles represent the mean area of the supporting tripods during the mean temporal mid-stance of the right middle legs. The orange lines in the xz-planes show the mean thorax length and orientation. The black asterisks represent the locations of the CoMs, which were calculated near the thorax-petiole joint at 20 % of the thorax length (McMeeking et al., 2012). The distance between the two asterisks represents the mean displacement of the ants for one stride cycle. The grey shaded contours represent individual sample ants on respective slopes during the temporal mid-stances of the right middle leg. All means were calculated from 15 strides per leg pair and slope resulting in 225 strides in total.
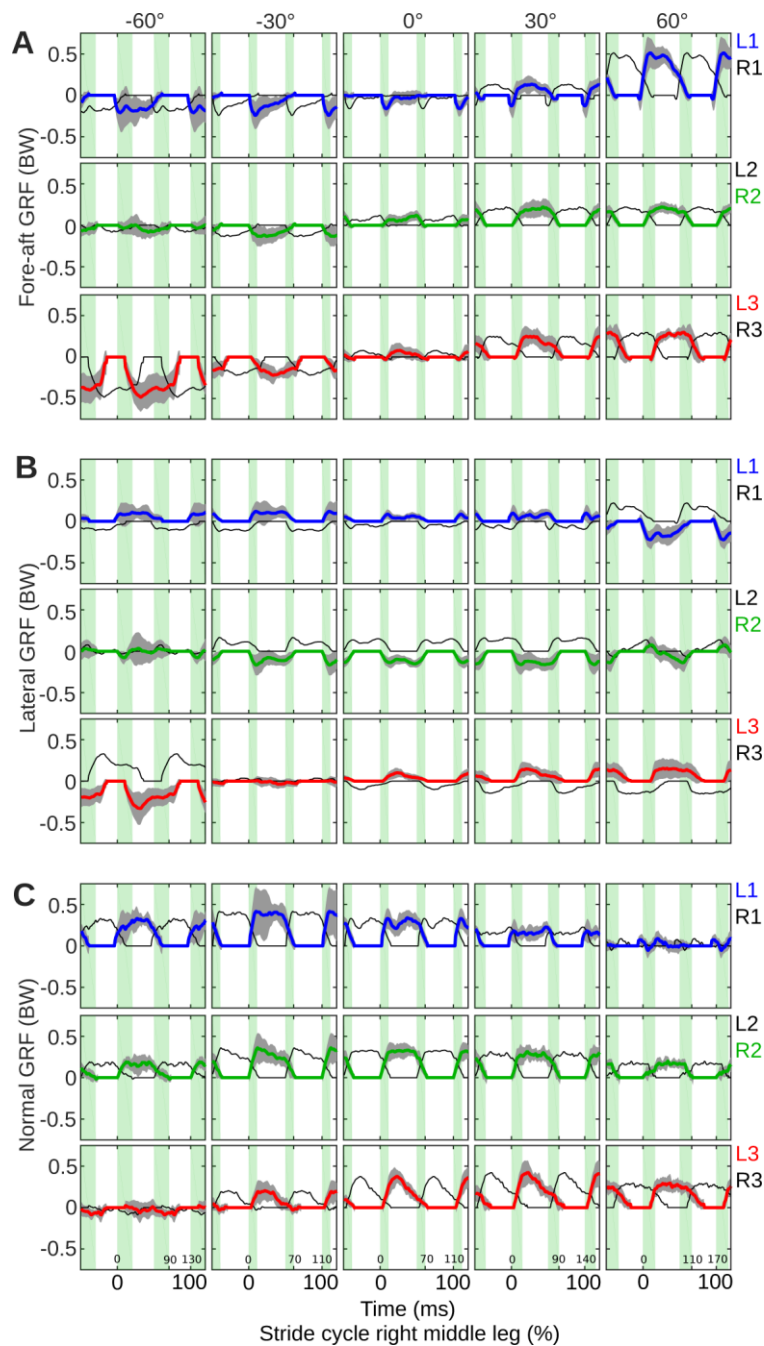
Fig. 3. GRF over time. (A) Fore-aft direction; (B) Lateral direction; (C) Normal direction. Mean GRF with standard deviations (grey shaded areas) over time and percentage of the stride cycle of the middle legs (N = 15 strides for each subset). The subplots are grouped by slopes and leg pairs (left front leg L1, right middle leg R2, left hind leg L3). The GRF signals are normalised to the mean stepping pattern of each slope (N=45 strides for each subset) and to the body weight BW (Table 3). The vertical green shaded areas mark the mean double support durations of the right middle leg (Fig. 7).
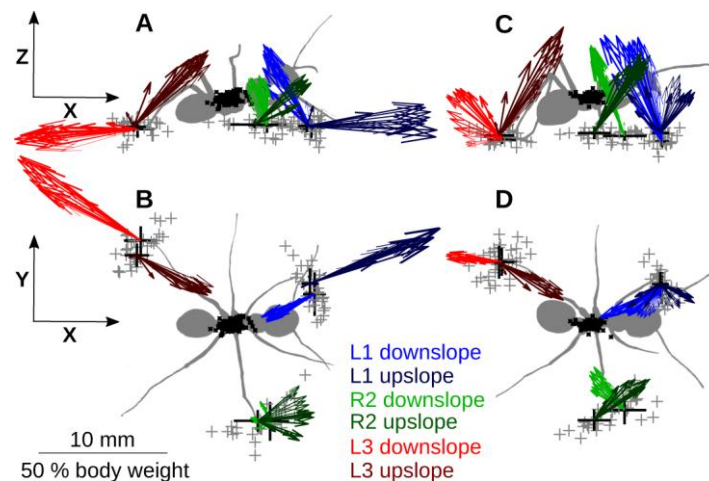
Fig. 4. Comparison of the mean GRF vectors on upslopes and downslopes. (A) Steep slopes, sagittal view. (B); Steep slopes, dorsal view; (C) Moderate slopes, sagittal view; (D) Moderate slopes, dorsal view. The mean GRF vectors (N=15 strides for each subset) are plotted in a space-fixed coordinate system for the left front legs (blue, L1), the right middle legs (green, R2) and the left hind legs (red, L3). Darker colours indicate the GRF on upslopes whereas lighter colours indicate the GRF on downslopes. The grey crosses represent the positions of the ground contacts of individual tarsi for all the strides (N=15 strides for each subset). The black crosses represent the mean positions with standard deviations of the grey crosses. The black dots illustrate the positions of petioles during temporal midstance of the right middle legs. The grey shaded contours represent sample ants during the temporal mid-stance of the right middle leg. The direction of progression is from left to right.
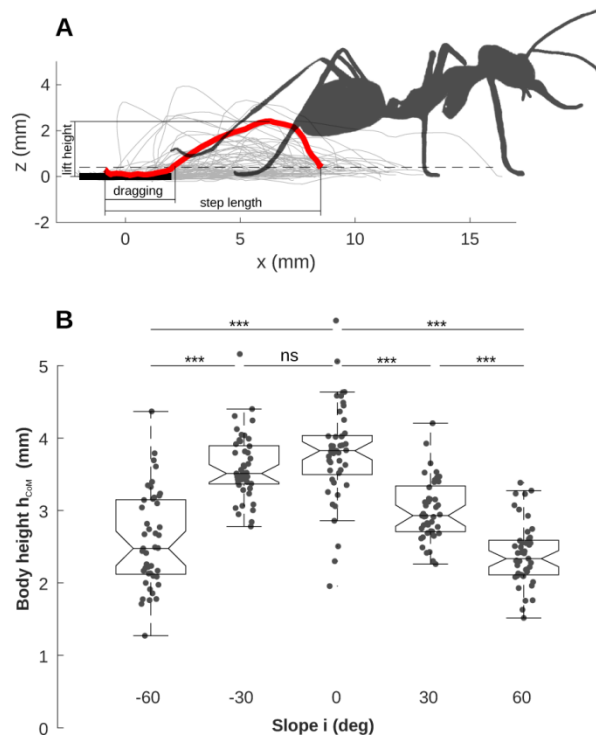
Fig. 5. Hind leg dragging and change of body height. (A) Dragging hind leg in the sagittal view. The dragging lengths are defined as the distances between the locations of touchdowns and the intersections of the hind leg tarsus trajectories (grey lines, N=75 strides) with the dashed horizontal line at twice of the measurement accuracy $z = 2 \cdot 0.2mm$. The red line highlights an example tarsus trajectory. The black bold horizontal line represents the location of the force plate. (B) Body height at different slopes. The body height was defined as the distance between CoM and substrate. The locations of the CoMs were calculated near the thorax-petiole joint at 20 % of the of the thorax length (McMeeking et al., 2012). p>0.05: ns; p≤0.05:*; p≤0.01:**; p≤0.001:***; two-sided Wilcoxon rank sum test with Bonferroni correction (N=45 per subset).
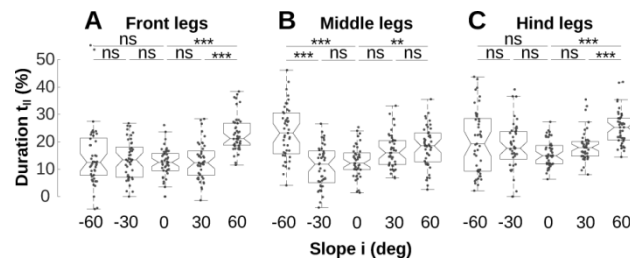
Fig. 6. Normalised double support durations for each leg pair at different slopes. The double support durations of the (A) Front legs, the (B) Middle legs and the (C) Hind legs were normalised by the stride durations of the middle legs (N=45 strides for each subset). The central lines of the Tukey boxplots are the medians and the edges of the boxes are the 25th and 75th percentiles. $p>0.05$: ns; $p\leq0.05$:*; $p\leq0.01$:**; $p\leq0.001$:***; two-sided Wilcoxon rank sum test with Bonferroni correction.